ACS APPLIED MATERIALS & INTERFACES

Research Article

Cite This: ACS Appl. Mater. Interfaces 2017, 9, 35516-35525

www.acsami.org

Tuning the Endocytosis Mechanism of Zr-Based Metal–Organic Frameworks through Linker Functionalization

Claudia Orellana-Tavra,[†,¶] Salame Haddad,[†,¶] Ross J. Marshall,[‡] Isabel Abánades Lázaro,[‡] Gerard Boix,[§] Inhar Imaz,[§] Daniel Maspoch,[§,⊥] Ross S. Forgan,*[,‡] and David Fairen-Jimenez*[,†]

[†]Adsorption & Advanced Materials Laboratory (AAML), Department of Chemical Engineering and Biotechnology, University of Cambridge, Philippa Fawcett Drive, Cambridge CB3 0AS, U.K.

[‡]WestCHEM School of Chemistry, University of Glasgow, Joseph Black Building, University Avenue, Glasgow G12 8QQ, U.K.

[§]Catalan Institute of Nanoscience and Nanotechnology (ICN2), CSIC and The Barcelona Institute of Science and Technology, Campus UAB, Bellaterra, 08193 Barcelona, Spain

[⊥]ICREA, Pg. Lluís Companys 23, 08010 Barcelona, Spain

Supporting Information

ABSTRACT: A critical bottleneck for the use of metal–organic frameworks (MOFs) as drug delivery systems has been allowing them to reach their intracellular targets without being degraded in the acidic environment of the lysosomes. Cells take up particles by endocytosis through multiple biochemical pathways, and the fate of these particles depends on these routes of entry. Here, we show the effect of functional group incorporation into a series of Zr-based MOFs on their endocytosis mechanisms, allowing us to design an efficient drug delivery system. In particular, naphthalene-2,6-dicarboxylic acid and 4,4′-biphenyldicarboxylic acid ligands promote entry through the *caveolin*-pathway, allowing the particles to avoid lysosomal degradation and be delivered into the cytosol and enhancing their therapeutic activity when loaded with drugs.

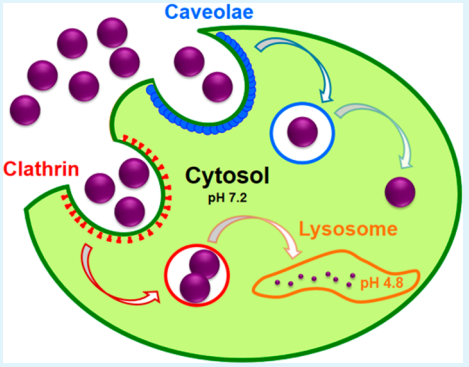

KEYWORDS: *metal–organic frameworks, metabolic pathways, drug delivery, endocytosis*

INTRODUCTION

Nanotechnology has attracted increasing interest over the past decades, especially in the field of medicine, where efforts have been directed toward the development of nanoparticulate drug delivery systems (DDSs) able to deliver drugs to specific cells. Nanoparticulate delivery vectors can overcome issues related to the use of free drugs such as their high toxicity, high and frequent doses, healthy tissue damage, nonspecific delivery, and short circulating half-lives.[1] Indeed, DDSs can maximize the bioavailability of the drug, both at specific places in the body and over time, by providing a slow release, specific targeting and delivery, and corresponding reduced toxicity, while maintaining the therapeutic effect of the cargo drug.[2,3] To date, several types of nanoparticles have been evaluated for drug delivery.[4] Among them, metal–organic frameworks (MOFs) have arisen as favorable candidates for this challenging application.[5−8] Their large pore volumes and surface areas, combined with their tunable surface chemistry and pore size, make them particularly interesting for drug delivery by allowing the selection and design of biocompatible and biodegradable systems. Several antiviral, anticancer, and antibacterial agents, as well as nucleic acids and biological gases, have been successfully entrapped in different MOFs.[9−15] In addition to the use of pristine MOFs, we recently proposed the use of amorphous MOFs for drug delivery.[16,17] By collapsing the MOFs' porosity around previously adsorbed drug molecules, release of the cargo can be extended from 2 to more than 30 days in the ∼200 nm systems that are able to cross the cellular membrane.

Optimal MOFs for drug delivery need to be versatile to load and deliver different compounds. However, one of the main limitations for translating MOFs to real drug delivery applications is the limited number of studies[18−20] detailing the penetration of MOF particles into cells. Indeed, an efficient MOF needs to be able to penetrate into cells and, more importantly, release its cargo molecules in the correct intracellular location. Although small molecules can enter cells by simple passive diffusion, nanoparticles generally require an energy-dependent process known as endocytosis, a mechanism present in all eukaryotic cells.[21,22] Importantly, the fate of the nanoparticles and hence their therapeutic effect after entering the cell is dependent on the endocytic pathways they enter through. However, no general guidelines for MOF particle internalization have been established to date due to the complexity of these mechanisms. All in all, endocytosis is an

Received: May 25, 2017
Accepted: September 19, 2017
Published: September 19, 2017

DOI: 10.1021/acsami.7b07342
ACS Appl. Mater. Interfaces 2017, 9, 35516−35525

Table 1. Colloidal Analysis of Nonloaded Zr-L1 Samples of Different Particles Sizes (i.e., $_{x}$Zr-L1) Alongside Functionalized (Zr-L2, Zr-L3, and Zr-L4) and Extended (Zr-L5 and Zr-L6) Derivatives as Well as Their Calcein Uptakes

		effective diameter (nm)[b]		polydispersity index		z-potential (mV)		
MOF	particle size (nm)[a]	PBS	growth media	PBS	growth media	water	growth media	calcein loading (wt %)
$_{50}$Zr-L1	50 ± 2	517 ± 40	238 ± 11	0.507	0.429	0.5	−9.5	2.7
$_{75}$Zr-L1	75 ± 3	575 ± 16	480 ± 21	0.581	0.479	12.3	−10.2	2.2
$_{92}$Zr-L1	92 ± 2	210 ± 2	161 ± 1	0.411	0.207	14.2	−11.2	2.2
$_{260}$Zr-L1	260 ± 21	328 ± 13	272 ± 12	0.295	0.167	18.9	−10.3	1.3
$_{652}$Zr-L1	652 ± 23	1637 ± 77	874 ± 105	0.373	0.262	8.52	−8.7	0.4
Zr-L2	211 ± 11/371 ± 38[c]	709 ± 13	237 ± 26	0.242	0.361	36.5	−8.7	0.4
Zr-L3	>400[d]	961 ± 16	596 ± 18	0.412	0.411	23.4	−10.4	0.3
Zr-L4	129 ± 19/266 ± 34[c]	828 ± 84	165 ± 1	0.282	0.151	42.7	−11.5	0.7
Zr-L5	78 ± 3	1319 ± 247	86 ± 13	0.392	0.397	8.0	−10.8	1.0
Zr-L6	115 ± 12/255 ± 14[c]	12 742 ± 3319	137 ± 25	0.488	0.445	−5.8	−8.8	6.3

[a]Measured by SEM. [b]Measured by DLS. [c]Two different populations of particle sizes were present. [d]Population too heterogeneous to determine particle size.

extremely cell dependent process, where several characteristics of the particles play a significant role in cellular uptake, such as size, shape, surface charge, and chemistry.[23,24]

The size of particles, and thus the size of the membrane invagination, gives a first natural way of classifying the different pathways that cells use to internalize particles. We can define macroscale endocytosis as phagocytosis and macropinocytosis. The former process relates to the ingestion of large particles (>0.5 μm) by specific types of cells such as neutrophils, monocytes, and macrophages.[25−27] Macropinocytosis is a nonspecific process that refers to the uptake of large amounts of extracellular fluid along with any particles present in it.[21] On the other hand, microscale endocytosis processes can be divided into three subgroups depending on the existence of protein coatings on the formed vesicles: (i) *clathrin*; (ii) *caveolae*; and (iii) *clathrin*- and *caveolae*-independent endocytosis.[27,28] *Clathrin*-mediated endocytosis is a specific pathway where receptors are responsible for cargo recognition, followed by the formation of *clathrin*-coated vesicles, which are usually up to 200 nm in size.[29] These vesicles merge with early endosomes, mature into late endosomes, and then fuse with lysosomes, leading to the hydrolysis of the DDS and its cargo, consequently nullifying its therapeutic effect.[30] *Caveolae*-mediated endocytosis on the other hand is associated with the formation of lipid raft-enriched flask-shaped invaginations coated with *caveolin*.[22,31] Particles internalized via *caveolae*-mediated endocytosis can be delivered later to different locations inside the cell. For instance, the formed vesicles can fuse with early endosomes and then with lysosomes for further degradation, as in the case of *clathrin*-mediated endocytosis. More interestingly, the particles internalized through this route can also be delivered to a pH neutral compartment called the caveosome and then transported to a final intracellular location, thus avoiding lysosomal degradation of the DDS and cargo.[32−34] Finally, other *clathrin*- and *caveolae*-independent endocytosis pathways are present in many cells; however, these are both less significant and less well understood than the previous cases.[22,35] To design new MOF-based DDSs capable of bypassing lysosomal degradation, it is critical to understand the factors determining which endocytosis pathway they go through.

We have previously reported the development of a complete methodology to study the pathways through which MOFs enter cells.[18] We demonstrated that particles of the Zr-based MOF UiO-66 (UiO, University of Oslo), 260 nm in size, were able to partially escape from endosomes and avoid acidic degradation in the lysosomes, whereas 150 nm particles were destroyed in these compartments. Indeed, lysosomes need to be circumvented to avoid cargo degradation due to the low pH and the presence of enzymes. Since the intracellular trafficking is affected not only by particle size but by the way DDSs interact with the membranes, we have tuned the surface chemistry of a family of Zr-based MOFs by including a series of functional groups on the organic ligands. We did not control/tune the particle size of these MOFs to avoid the presence of modulators that could affect the surface chemistry, but included a range of UiO-66 MOFs with different particle size for comparison. We report the effect of linker functionalization (and subsequent changes to the outer surfaces) of the MOFs on endocytosis pathways and efficiency, and use this information to prepare an optimal DDS with enhanced endocytosis efficacy and improved ability to avoid lysosomal entrapment.

RESULTS AND DISCUSSION

Zirconium-based MOFs are a promising option for drug delivery applications due to their low toxicity,[36] with UiO-66 showing an IC_{50} value of 1.50 ± 0.15 mg/mL after 24 h of exposure.[16] The structure of this well-studied MOF contains Zr-oxo clusters connected by bridging BDC linkers to give an overall composition $[Zr_6O_4(OH)_4(BDC)_6]_n$ (where BDC = 1,4-benzene dicarboxylate), with large porosity (S_{BET} = 1200 m^2 g^{-1}, V_p = 0.5 cm^3 g^{-1}) and two cavities (with diameters of ca. 8 and 11 Å).[16,37−39] To find a MOF with optimal endocytic characteristics, we first prepared a series of UiO-66 samples with different particles sizes: 50, 75, 92, 260, and 652 nm; we named these structures $_{x}$Zr-L1, where x is the particle size (see Table 1). Second, we prepared a range of UiO-66-like materials with different surface chemistries by substituting the original BDC linker with functionalized linkers as well as extended linkers.[40,41] Scheme 1 shows the six different linkers (L1−L6) utilized to build the Zr-based MOFs (herein termed Zr-L1 to Zr-L6). L1 is BDC, used for UiO-66; L2−L4 are BDC functionalized with -Br, -NO_2, and -NH_2, respectively; and L5 and L6 (naphthalene-2,6-dicarboxylic acid and 4,4′-biphenyldicarboxylic acid, respectively) are extended linkers.

We loaded the fluorescent molecule calcein into all the MOFs to allow their intracellular detection using flow cytometry and confocal microscopy. We selected calcein

DOI: 10.1021/acsami.7b07342
ACS Appl. Mater. Interfaces 2017, 9, 35516−35525

Scheme 1. Organic Linkers Used To Synthesize Zr-Based MOFs

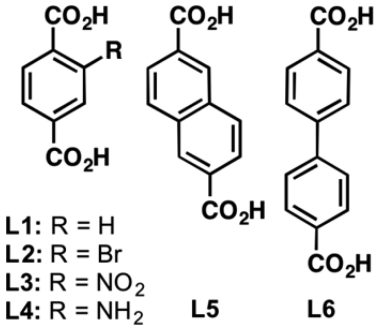

because of its hydrophilic character, which makes it unable to cross the cell membrane and thus requires a DDS to be transported through it.[17,42] We have previously studied the release of calcein from all the MOFs in PBS, confirming that leakage of the dye is similar for all of them.[17] Figure S1 presents the powder X-ray diffraction (PXRD) patterns for the synthesized MOFs compared with the patterns predicted from single crystal structures. Figure S2 shows the scanning electron microscopy (SEM) images of the $_x$Zr-L1 MOFs and of the functionalized derivatives. Table 1 shows the particle sizes, ranging from 50−652 nm for Zr-L1 and from 78 to >400 nm for Zr-L2−Zr-L6 (obtained from the SEM images). Since the physicochemical properties of MOFs, and of nanoparticles in general, are affected by the media in which they are present, we determined their colloidal properties: hydrodynamic size in PBS and growth media, z-potential in water and growth media, all at pH 7.4. The zeta potential is the effective surface potential at the hydrodynamic "shear surface" close to the solid−liquid interface. It determines the electrostatic repulsion between particles, or between particles and a surface such as a cell membrane, that acts to promote or prevent particle attraction and adhesion. We expect that the different surface functionalities with differing charges will affect the surface properties and hence the colloidal and uptake properties of the MOF particles. Table 1 shows the hydrodynamic diameter of all the analyzed MOFs in PBS and growth media. The degree of aggregation was much more pronounced in PBS than in growth media, for example, the hydrodynamic diameter of Zr-L6 is two orders of magnitude less in growth media compared to PBS. The hydrodynamic diameter in growth media indicate aggregation is only significant for the smaller particle size Zr-L1 samples. We also observed a decrease in the polydispersity index, which ranged from 16% for $_{50}$Zr-L1 to 50% for $_{92}$Zr-L1. MOFs are susceptible to aggregation in aqueous solvents due to their varying hydrophobicities.[37] However, the formation of a "protein corona"[43] on the external surface of the MOF particles, resulting from the adsorption of different kinds of proteins from the growth media, might be the reason for their lower susceptibility to aggregation compared to PBS and also the negative zeta potentials measured in media compared to water.

The amounts of calcein loaded in all the MOFs, with values ranging between 0.3 and 6.3 wt % for Zr-L3 and Zr-L6, respectively, are presented in Table 1. For Zr-L1, the amount of loaded calcein decreases with increasing particle size. Since smaller particles have higher external surface areas compared with larger particles, this suggests that calcein mostly adsorbs on the external surface or to potential superficial defects or roughness. In the case of the functionalized MOFs (i.e., Zr-L2−L4), the loading values are generally lower compared to the nonfunctionalized $_x$Zr-L1 particles, even for particles similar in size such as $_{260}$Zr-L1 (260 nm; 1.3 wt %) and Zr-L4 (266 nm; 0.7 wt %). In the case of Zr-L6, that is, the MOF with the longest linker and therefore largest cavities, the amount increased to ∼6 wt %, suggesting some additional adsorption in the internal porosity as well as the outer surface. In all cases, loading values were sufficiently high to detect the MOFs through flow cytometry and confocal microscopy.

Uptake Efficiency of Zr-L1 with Different Particle Sizes. The MOFs with different linker functionalities included in our study also present different particle sizes. To be able to discriminate between the role of surface chemistry and particle size on the endocytosis pathways and uptake efficiencies, we split the analysis to study both effects separately. As a reference for the surface chemistry analysis, we first investigated the effect of the particle size on the uptake of Zr-L1 using a broad range of sizes. Figure 1 shows the normalized intracellular fluorescence, measured by flow cytometry, of HeLa cells incubated for 1.5 h with $_x$Zr-L1 with different particles sizes. We chose the mass ratio of the different MOFs in such a way as to keep the amount of calcein constant and used an equal amount of free calcein as a control. $_{50}$Zr-L1 presented the highest intracellular fluorescence, and therefore, we normalized all the values against it. Although calcein is considered an impermeable dye, a low calcein uptake was observed, 17% in comparison with $_{50}$Zr-L1 uptake. We have seen this effect for calcein previously, and it has also been observed for other impermeable dyes, which are internalized by endocytosis.[16,18,44] In general, there seems to be a trend of uptake efficiency decreasing with increasing particle size. In the case of $_{652}$Zr-L1, the amount of calcein entering the cell is not significantly different from free calcein, showing that very little MOF is entering the cell, likely due to its large size.

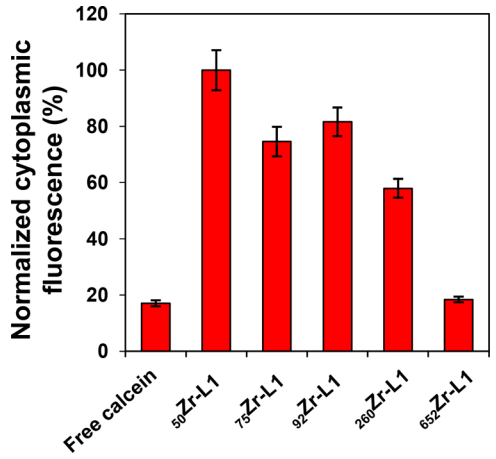

Figure 1. Normalized intracellular fluorescence of HeLa cells incubated with Zr-L1 of different particle sizes. We used different concentrations of each MOF to keep the amount of calcein constant.

In flow cytometry, cells or particles passing through the laser beam scatter light, which is detected as forward scatter (FS) and side scatter (SS). FS correlates with cell size and SS is proportional to the granularity of the cells. In this manner, healthy cell populations can often be identified based on size and granularity alone. The fact that $_{652}$Zr-L1 is not entering the cells is confirmed by the change in the SS versus FS plot when cells are incubated with $_{652}$Zr-L1 (Figure 2); HeLa cells with

DOI: 10.1021/acsami.7b07342
ACS Appl. Mater. Interfaces 2017, 9, 35516−35525

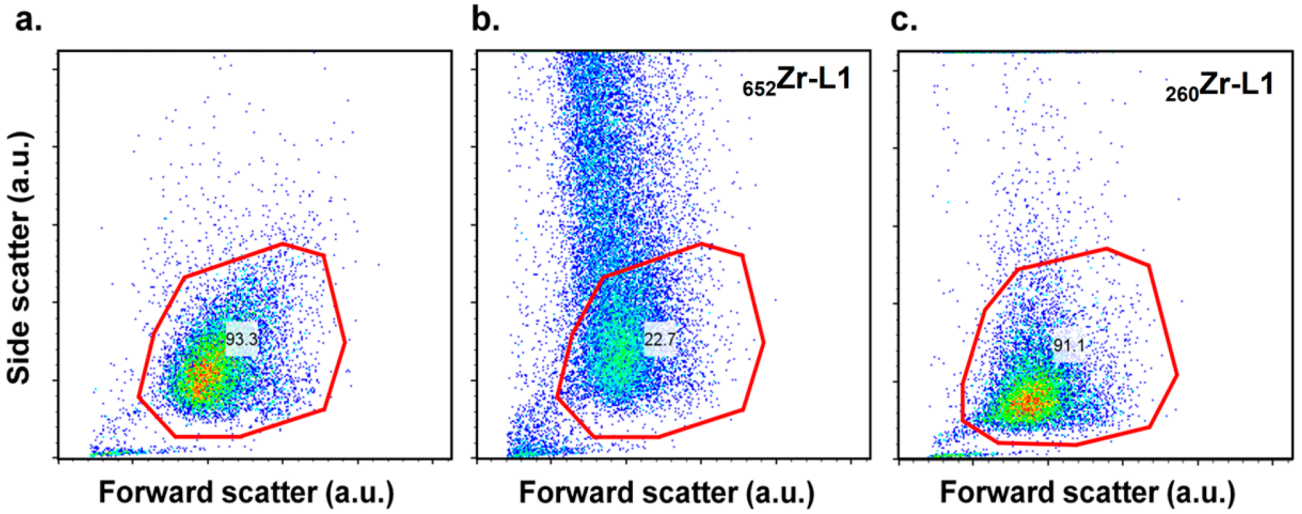

Figure 2. Side scatter versus forward scatter plot obtained from fluorescence-activated cell sorting (FACS) of (a) HeLa cells, (b) HeLa cells incubated with $_{652}$Zr-L1, and (c) HeLa cells incubated with $_{260}$Zr-L1. Solid red line shows the gate around morphologically normal HeLa cells. The numbers indicate the percentage of cells within that gate.

normal size and granularity mostly fall within the gate seen in Figure 2a (93.3%). When cells are incubated with $_{652}$Zr-L1, there is a significant increase in side scatter (Figure 2b), indicating an increase in granularity due to MOFs adhered to the outside of cells. Only 22.7% of cells remain in the gate where healthy HeLa cells should be, and within this population there is very little detectable fluorescence, indicating that very little MOF is taken up by cells. In contrast, cells incubated with $_{260}$Zr-L1 have normal side scatter (Figure 2c), with 91.1% of cells falling within the gate, indicating that the granularity of the cells is normal and hence that there is no MOF stuck on the outer cellular membrane.

Influence of Different Endocytosis Inhibitors on the Cellular Uptake of Zr-L1. We studied the endocytic pathways (*clathrin*, *caveolae*, and *clathrin*- and *caveolae*-independent endocytosis) for the internalization of Zr-L1 by HeLa cells using different pharmacological inhibitors. First, we used sucrose and chlorpromazine to independently inhibit *clathrin*-mediated endocytosis. Sucrose plays a role in the scattering of *clathrin* matrices on the cell membrane, whereas chlorpromazine inhibits *clathrin*-coated pit formation by reversibly translocating *clathrin* and its adaptor proteins from the plasma membrane to intracellular vesicles.[26,45] Second, we used nystatin, a polyene antibiotic that sequestrates cholesterol molecules from the cell membrane, to inhibit *caveolae*-mediated endocytosis.[45] Finally, we used rottlerin to hinder *macropinocytosis* by inhibiting kinase proteins.[46] To evaluate the efficacy of these inhibitors we used specific tracers of the endocytic pathways: transferrin, ceramide and dextran for *clathrin*- and *caveolae*-mediated endocytosis, and *macropinocytosis*, in turn.[26,47] Since the inhibition of one particular endocytic pathway may trigger compensatory uptake mechanisms with time,[45] we assessed the internalization of the particles after a short exposure time to the endocytosis inhibitors (ca. 2 h).

Figure 3 shows HeLa cells' internal fluorescence after incubation with $_{x}$Zr-L1 in the presence of the different endocytic inhibitors; Table S1 shows the values for each sample. To determine if the differences were statistically significant, we compared every value to the control at 37 °C using one-way analysis of variance (ANOVA) followed by

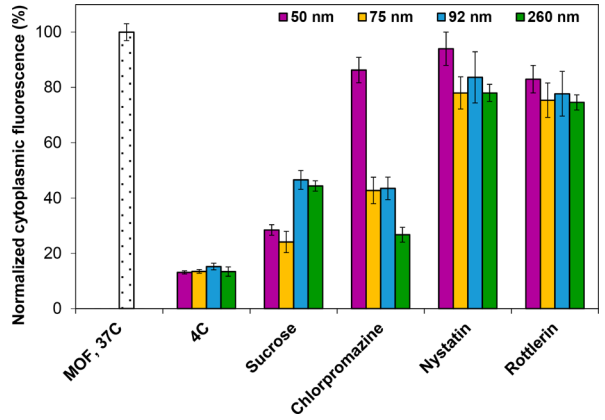

Figure 3. Effects of pharmacological endocytosis inhibitors on the uptake of Zr-L1 with different particle sizes, measured by flow cytometry.

Dunnett's test to adjust for multiple comparisons (Table S2). Cellular uptake of the MOFs was significantly reduced by ~85% when cells were incubated at 4 °C. At this temperature, the metabolic activity of a cell is significantly reduced,[45] confirming that the particles were taken up by energy-dependent endocytosis and not by passive diffusion. For $_{50}$Zr-L1, particle uptake decreased significantly to 29% when cells were treated with hypertonic sucrose. Despite the fact that sucrose is considered an inhibitor of *clathrin*-mediated endocytosis,[48,49] there is evidence suggesting that it has some effect on non-*clathrin*-mediated endocytosis pathways.[50] For this reason, we used chlorpromazine to reconfirm the sucrose result as there is no evidence that it affects *caveolae*-mediated endocytosis or other endocytic pathways.[45] For chlorpromazine, the uptake decreased only moderately to 86%, although this was not statistically different from the control at 37 °C. The fact that sucrose affects uptake while chlorpromazine does not suggests that the main uptake routes of $_{50}$Zr-L1 do not involve *clathrin*-mediated pathways, and that, in this case, sucrose is inhibiting non-*clathrin*-mediated endocytosis pathways. Similarly, $_{50}$Zr-L1 particle uptake moderately decreased to 94 and 83% when cells were treated with nystatin and rottlerin

DOI: 10.1021/acsami.7b07342
ACS Appl. Mater. Interfaces 2017, 9, 35516−35525

respectively, again, this was not statistically different from the control at 37 °C. This indicates that the main routes of entry of $_{50}$Zr-L1 do not involve *clathrin*- or *caveolae*-mediated endocytosis, or macropinocytosis, but *clathrin*- and *caveolae*-independent endocytosis. For $_{75}$Zr-L1 and $_{92}$Zr-L1, similar levels of inhibition by chlorpromazine, nystatin, and rottlerin were observed, decreasing to ∼45, 84, and 78%, respectively, for both MOFs. However, the signals for these MOFs when treated with nystatin and rottlerin were not statistically significantly different from the control, indicating that they mainly enter the cell through *clathrin*-mediated endocytosis. In the case of $_{75}$Zr-L1, the decrease when treated with nystatin and rottlerin was slightly greater than that observed for $_{92}$Zr-L1 and showed some statistical significance, suggesting perhaps some uptake by *caveolae*-mediated endocytosis and macropinocytosis. For $_{260}$Zr-L1, the decrease in fluorescence intensity when treated with nystatin and rottlerin was the same as $_{75}$Zr-L1 (down to 78% and 75% respectively) and was statistically significant. However, an even larger decrease in intensity was observed for chlorpromazine, suggesting that, for $_{260}$Zr-L1, *clathrin*-mediated endocytosis again dominates.

The decrease in internal fluorescence when using chlorpromazine is different than what we obtained in our previous work for similar particle size.[18] The discrepancy comes from the different synthesis protocol and modulators used: HCl and benzoic acid versus acetic acid here. The colloidal stability and properties of UiO-66 are highly dependent on the modulator conditions utilized in the synthesis. This is due to the fact that modulators at higher concentrations and lower pK_a lead to the formation of more defects in the crystals, which in turn alter the surface chemistry of UiO-66 and enhance its colloidal stability.

Table 2 summarizes the statistical significance for comparison between the intracellular fluorescence of the different MOFs treated with a given inhibitor. The results show that there is no statistically significant difference between the normalized intracellular fluorescence of the Zr-L1 MOFs of different sizes when treated with nystatin (i.e., for *caveolae*) and rottlerin (i.e., *macropinocytosis*). This is despite the fact that Table S2 shows that decreases in fluorescence for $_{75}$Zr-L1and $_{260}$Zr-L1 with these inhibitors are statistically significant when compared to the control at 37 °C. In general, it seems that particle size of the materials included in this study does not greatly affect the uptake pathway. A minor difference is found for $_{75}$Zr-L1, and more significantly for $_{260}$Zr-L1, which exhibit some endocytosis by the *caveolin*-mediated pathway, and in doing so avoid degradation in the lysosomes.

Table 2. Comparison of Normalized Internal Fluorescence of HeLa Cells Treated with Each MOF and Different Pharmacological Inhibitors[a]

MOF vs MOF	sucrose	chlorpromazine	nystatin
	clathrin	clathrin	caveolae
$_{50}$Zr-L1 vs $_{75}$Zr-L1	ns	**	ns
$_{50}$Zr-L1 vs $_{92}$Zr-L1	**	**	ns
$_{50}$Zr-L1 vs $_{260}$Zr-L1	**	***	ns
$_{75}$Zr-L1 vs $_{92}$Zr-L1	*	ns	ns
$_{75}$Zr-L1 vs $_{260}$Zr-L1	**	*	ns
$_{92}$Zr-L1 vs $_{260}$Zr-L1	ns	*	ns
Zr-L2 vs Zr-L3	ns	ns	ns
Zr-L2 vs Zr-L4	ns	**	ns
Zr-L3 vs Zr-L4	ns	**	ns
Zr-L2 vs Zr-L5	**	****	***
Zr-L2 vs Zr-L6	***	****	****
Zr-L3 vs Zr-L5	**	****	**
Zr-L3 vs Zr-L6	***	****	**
Zr-L4 vs Zr-L5	**	****	***
Zr-L4 vs Zr-L6	***	****	***
Zr-L5 vs Zr-L6	ns	ns	ns

[a]Statistical significance, determined by unpaired *t* test (no significance, ns, $P > 0.05$, *$P \le 0.05$, **$P \le 0.01$, ***$P \le 0.001$, ****$P \le 0.0001$). Rottlerin (macropinocytosis) has not been included because all the results show no significance.

Internalization Efficiency of Zr-Based MOFs with Different Surface Chemistry. Following the analysis of the role of particle size on the internalization of the MOF particles, we continued with the MOFs with different surface chemistries. As mentioned above, the particle size of these MOFs ranged from 78 to more than 400 nm, for Zr-L5 and Zr-L3, respectively. Figure 4 presents the normalized internal

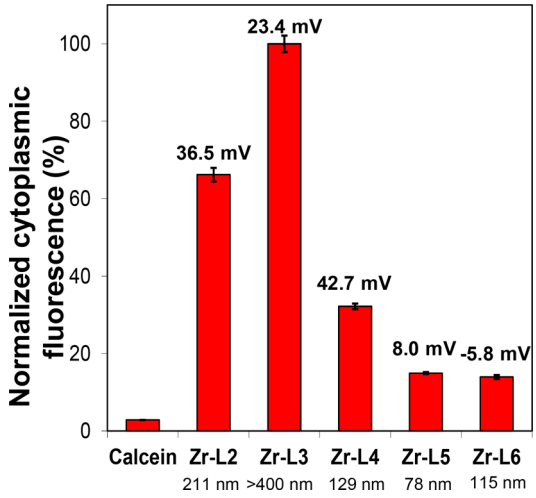

Figure 4. Normalized intracellular fluorescence of HeLa cells incubated with Zr-L2 to Zr-L6. We used different calcein concentrations as controls for each MOF so that they were equivalent to the loaded amount in the respective MOF; z-potential values shown at top of bars, particle size at the bottom.

fluorescence of HeLa cells after treatment for 1.5 h with the functionalized MOFs, Zr-L2 to Zr-L6 (0.5 mg/mL), or free calcein (equivalent to the same amount loaded in each MOF for normalization purposes). We considered the highest value as 100%, which corresponded to Zr-L3. Among all the MOFs, Zr-L3 was internalized more efficiently than any of the others, followed by Zr-L2 then Zr-L4. The less efficient MOFs were Zr-L5 and Zr-L6. Interestingly, we did not observe the same trend of decreasing efficiencies with increasing particle sizes that we found with $_x$Zr-L1 samples, confirming the importance of surface chemistry. This is further confirmed by noting that for $_x$Zr-L1 particles the variability in the uptake efficiency is low (with the exception of $_{650}$Zr-L1, which is too large to be taken up), whereas for Zr-L2 to Zr-L6 the variability is much larger.

For the MOFs with functionalized ligands (i.e., −Br, −NO_2, and −NH_2, for Zr-L2, Zr-L3, and Zr-L4, respectively), cellular uptake seems to be inversely related to zeta potential (Table 1). Zr-L3, which has the highest uptake, has a zeta potential of 23.4 mV, followed by Zr-L2 (36.5 mV) and Zr-L4 (42.7 mV). The MOFs with extended linkers (i.e., Zr-L5 and Zr-L6) have low zeta potentials of 8.0 and −5.8 mV, respectively, which might

DOI: 10.1021/acsami.7b07342
ACS Appl. Mater. Interfaces 2017, 9, 35516−35525

explain why they are not significantly taken up by the cells. Indeed, it has been reported that surface charge has a critical role in cellular uptake and drug delivery systems, where positive charged nanoparticles show higher uptake efficacy.[51] The reason for this is the higher attraction of cationic NPs could be related to the negatively charged plasma membrane of cells.[52,53] Interestingly, we can see that the zeta potential values for all the MOFs in media converge to around −10 mV, which is the zeta potential measured for growth media. This confirms the "protein corona" formation around the external surface of the particles.

Influence of Endocytosis Inhibitors on the Cellular Uptake of Zr-Based MOFs with Different Surface Chemistry. After the analysis of the endocytosis efficiency, we then moved to study the different endocytic pathways. Figure 5 shows HeLa cells' internal fluorescence after

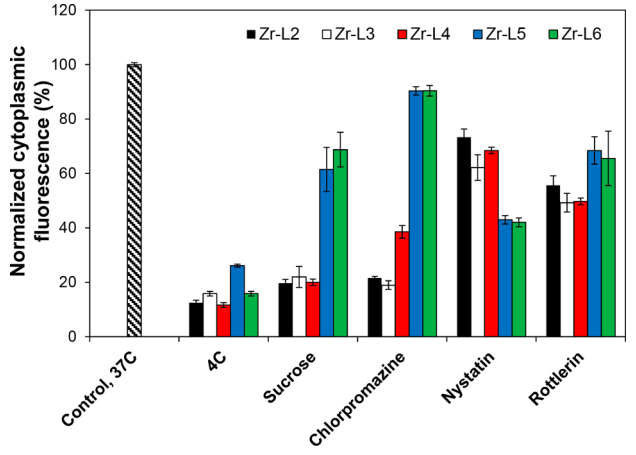

Figure 5. Effects of pharmacological endocytosis inhibitors on the uptake of Zr-based family MOFs, measured by flow cytometry.

incubation with each MOF (0.5 mg/mL) in the presence of different endocytic inhibitors. The uptake of all the MOFs was highly inhibited at 4 °C, between 74 and 88% lower than the corresponding control at 37 °C. On the basis of the results, and as with the endocytosis efficiency discussed above, it was possible to segregate the MOFs into two subgroups regarding the endocytosis pathways used by cells for their internalization: (i) MOFs with functional groups, and (ii) MOFs with extended linkers. On one hand, the uptake of Zr-L2, Zr-L3, and Zr-L4 decreased to values close to 20% after incubation with sucrose and chlorpromazine (i.e., *clathrin*-mediated endocytosis inhibitors), whereas exposure to nystatin (i.e., *caveolae*-mediated endocytosis inhibitors) had a moderate effect of ∼70%, and rottlerin (i.e., *macropinocytosis* inhibitor) reduced the uptake to ∼48%. On the other hand, the uptake of Zr-L5 and Zr-L6 was greatly inhibited when *caveolae*-mediated endocytosis was blocked by nystatin, decreasing to ∼42%. Inhibition of *clathrin*-mediated endocytosis on these systems only had a moderate effect, decreasing to ∼65 and 90% for sucrose and chlorpromazine, respectively. Inhibition with chlorpromazine showed no statistical significance with respect to the controls for both Zr-L5 and Zr-L6. Rottlerin decreased the uptake of these two MOFs to ∼67%. As observed above for $_x$Zr-L1 samples, in some cases the effect of sucrose on the MOF uptake was more dramatic than chlorpromazine due to pathways other than *clathrin*-mediated routes being blocked.[45,50] The literature offers conflicting data about the selection of endocytic pathways for charged particles, probably because the process is cell-specific. However, studies on Hela cells using charged NPs support *clathrin*-mediated endocytosis for positively charged particles, and *clathrin*-independent for negatively charged ones.[54,55] This may explain why Zr-L6, negatively charged, is internalized mainly through *caveolae*-mediated endocytosis.

Table 2 shows the comparison of the normalized internal fluorescence values for each MOF with the others after exposure to the inhibitors, allowing the statistical differences within these two subgroups and between them to be determined. First, the only significant difference ($P \leq 0.01$) within the group of functionalized MOFs (Zr-L2, Zr-L3, and Zr-L4) was between Zr-L4, and Zr-L2 and Zr-L3, when treated with chlorpromazine. We did not observe any significant difference between these three MOFs when treated with nystatin or rottlerin. The same was true in the case of the subgroup of extended linkers, that is, Zr-L5 and Zr-L6, where we did not observe any significant difference within them, for any inhibitor used. Conversely, there were significant differences when we compared the values for the functionalized MOFs, Zr-L2, Zr-L3, and Zr-L4, with the values for Zr-L5 and Zr-L6, for sucrose, chlorpromazine, and nystatin. This result confirms that the cellular uptake behavior is different between the two subgroups (MOFs with functionalities vs MOFs with extended linkers). The size of the particles could play a minor role in inter- and intragroup differences, as we have seen that the cell uptake behavior is less affected by a change in the size of Zr-L1 in comparison to the surface chemistry of the MOFs, which is greatly affecting these processes. However, more importantly, the surface chemistry of the particles is affecting these processes. The two subgroups of MOFs can also be segregated with respect to zeta potential. The MOFs with functionalities (Zr-L2 to Zr-L4) have zeta potentials in the range of 23.4−42.7 mV, while the MOFs with extended linkers (Zr-L5 and Zr-L6) have low zeta potentials of 8.0 and −5.8 mV, respectively. MOFs with functional groups and thus higher zeta potentials undergo preferably *clathrin*-mediated endocytosis, and the MOFs with extended linkers and thus low surface charge are internalized mostly through *caveolae*-mediated endocytosis. $_x$Zr-L1 particles do not have functional groups, but their surface charge is slightly greater than Zr-L5 and Zr-L6, which might be due to the higher surface density of clusters on their surface compared to the MOFs with extended linkers. The high propensity of UiO-66 to have defects might also play a role in increasing the surface charge.[56] This can explain why $_x$Zr-L1 particles, with a surface charge between that of the functionalized MOFs and that of the extended linker MOFs, go through *clathrin*-mediated endocytosis in addition to *caveolae*-mediated endocytosis, whereas Zr-L5 and Zr-L6 only go through *caveolae*-mediated endocytosis. It is noteworthy that all MOFs are also internalized by *macropinocytosis* as it is a nonselective process carried out by cells.

Influence of the Uptake Pathway on the Final Fate of Zr-Based Family MOFs, Colocalization Studies. Depending on the type of endocytosis, the internalized carrier and loaded molecules are transported through different metabolic pathways. They are then processed, contained in vesicles, to their final intracellular destination.[57] As explained above, particles that undergo *caveolae*-mediated endocytosis can potentially bypass lysosomal acidic degradation. Studies on viruses and bacteria provide strong evidence that they are internalized through this pathway, and they are able to avoid digestion in the lysosomes.[58] On the basis of this, one can

DOI: 10.1021/acsami.7b07342
ACS Appl. Mater. Interfaces 2017, 9, 35516−35525

expect that MOFs would have a higher chance of avoiding the lysosome and, thus, delivering their cargo in other intracellular locations if they are internalized by *caveolae*-mediated endocytosis, for example, Zr-L5 and Zr-L6. We consequently investigated the intracellular fate of the MOFs after the endocytosis process, in particular, by examining whether the MOFs were found in lysosomes for further acidic degradation. For this purpose, we used confocal fluorescence microscopy to determine if the particles were in the same intracellular location as a lysosome marker, LysoTracker-Deep Red. We also measured the Manders' overlap coefficient (MOC), which varies from 0 to 1 for nonoverlapping and complete colocalization, respectively.[59,60] Figure 6a shows the images obtained from confocal microscopy of HeLa cells incubated with each MOF and LysoTracker-Deep Red. At 2 h, we observed a high degree of colocalization between Zr-L2, Zr-L3, Zr-L4, and LysoTracker-Deep red, which is illustrated by the yellow color in the merged images. In the case of Zr-L5 and Zr-L6, we found only a moderate correlation between the MOFs and LysoTracker-Deep Red, which was confirmed by quantification analysis using MOC (Figure 6b). It was again possible to identify the two subgroups of MOFs: (i) Zr-L2, Zr-L3, and Zr-L4; and (ii) Zr-L5 and Zr-L6. Within the first subgroup, all the MOFs behave in the same way (average MOC ca. 0.8, with no statistically significant difference between them); the same occurs with the second subgroup (average MOC ca. 0.4, with no statistically significant difference). By comparing the two subgroups, the colocalization degree of Zr-L5 and Zr-L6 was on average ~50% lower than that of Zr-L2 to Zr-L4 (Table S3 shows the statistical analysis of the MOC for each MOF compared with the others). This result indicates that Zr-L2, Zr-L3, and Zr-L4 are mostly localized in lysosomes for further acidic degradation, whereas a significant quantity of Zr-L5 and Zr-L6 may be able to successfully avoid it and potentially release the cargo in the cytosol or other organelles.

On the basis of all these results, we can see correlations of both the particle size and linker functionalities (and thus surface chemistry) with the uptake efficiency and final fate of the MOFs inside cells. Without a doubt, overall uptake efficiency is an important feature, but MOFs entrapped in endosomes or lysosomes do not contribute to the final aim of delivering drugs in the cytosol and so this may lead to a reduced therapeutic effect. For instance, this is the case of Zr-L3, which is the most successful MOF in terms of cellular uptake; however, after the endocytosis process, it was found in the lysosomes for further degradation. In contrast, Zr-L5 and Zr-L6 were the least efficient in terms of cellular uptake; however, they could avoid the lysosomes and potentially deliver their cargo in the cytosol with an improved therapeutic result.

We have previously investigated the cytotoxicity of Zr-L1 to Zr-L6 loaded with α-cyano-4-hydroxycinnamic acid (α-CHC) and found α-CHC@Zr-L6 to be more toxic than α-CHC@Zr-L1.[17] With our newly acquired knowledge of the endocytosis pathways, we are able to rationalize these results (reproduced in Figure 7) in more depth. We did not find any significant difference in viability for cells treated with empty and α-CHC-loaded Zr-L1 to Zr-L5, with viability remaining above 80% for both conditions at any given concentration of MOF (data for Zr-L1, Zr-L3, and Zr-L6 are shown in Figure 7). Empty Zr-L6 is also noncytotoxic at the concentrations used. α-CHC@Zr-L6, however, decreases the viability down to 59 ± 5% at a MOF concentration of 1 mg mL^{-1}. This once again confirms that even though Zr-L3 is more efficient than Zr-L6 at delivering cargo into the cell, it is less therapeutically effective than the latter since most of the cargo ends up being degraded in the lysosomes. A comparison of Zr-L1 and Zr-L6 also confirms that it is not necessarily the amount of drug loaded in the MOF that

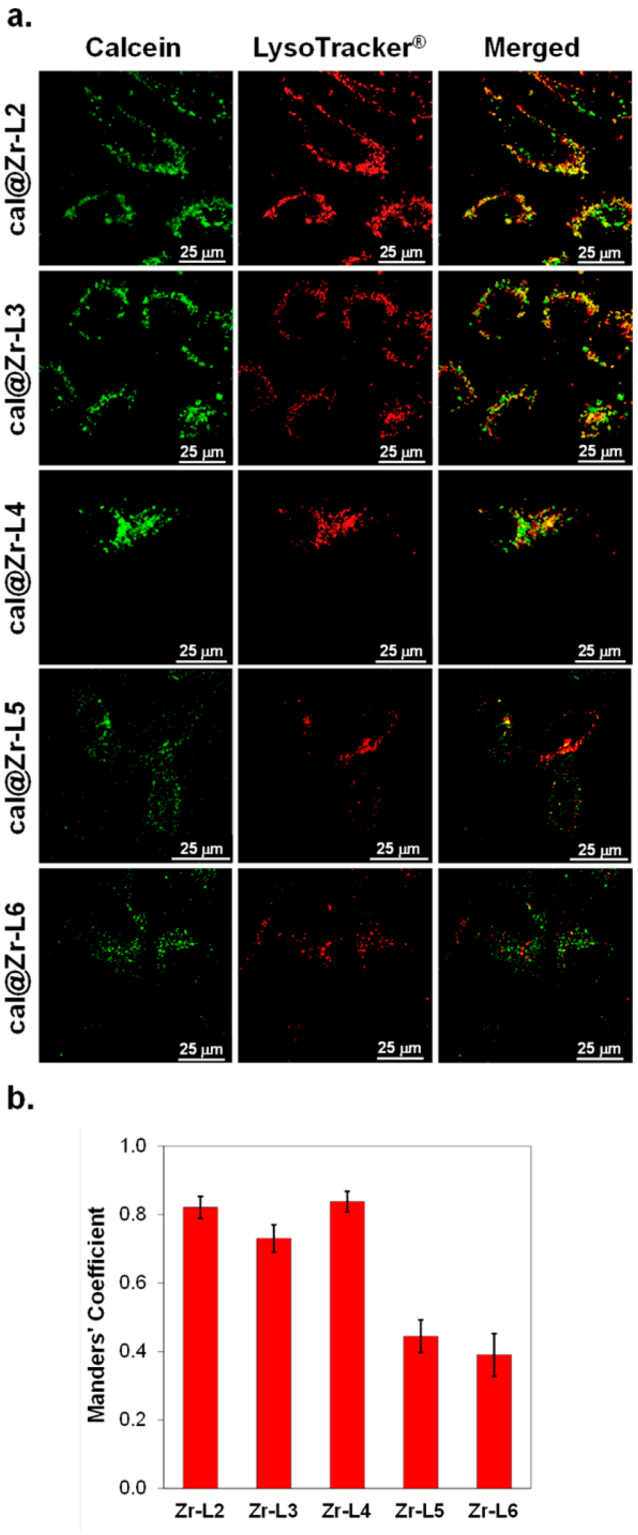

Figure 6. (a) Confocal microscopy images of HeLa cells incubated with Zr-based MOFs loaded with calcein (green fluorescence, i.e., calcein), and LysoTracker-Deep red (red fluorescence), for 2 h. (b) Manders' overlapping coefficient for all the MOF samples and the lysosome marker. Error bars represent the standard error of at least 10 independent images.

DOI: 10.1021/acsami.7b07342
ACS Appl. Mater. Interfaces 2017, 9, 35516−35525

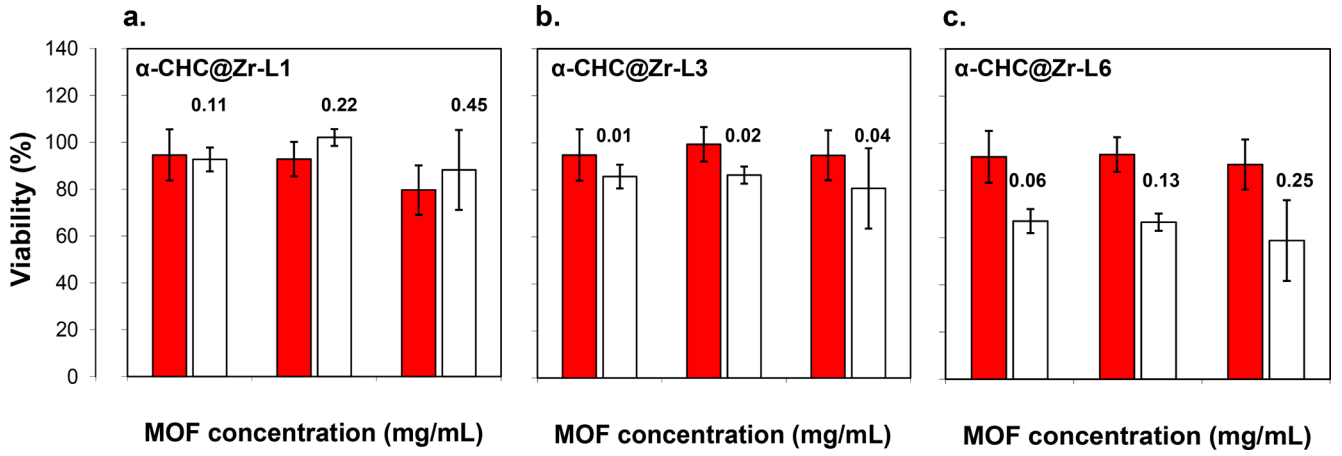

Figure 7. MTS viability assay of (a) α-CHC@Zr-L1, (b) α-CHC@Zr-L3, and (c) α-CHC@Zr-L6.[17] Red and white bars correspond to empty and loaded MOF, respectively. The concentration of MOF in the loaded samples was maintained the same as the empty MOFs (0.25, 0.5, and 1 mg/mL) to allow for comparison. Numbers on top of the bars indicate the concentration of α-CHC in mg/mL corresponding to the MOF concentration used.

determines its efficacy, given that Zr-L1, which has a higher loading than Zr-L6, is still less effective at killing cells.

CONCLUSIONS

We have synthesized a range of Zr-based MOFs of different sizes and with different surface chemistries and showed, using the fluorescent molecule calcein, that they enter cells through different endocytic pathways. We have demonstrated that control of surface chemistry, in this case through linker functionalization, is critical to tune the pathways in which cells take up particles, whereas particle size does not exert a great influence here. We showed that Zr-L1 (nonfunctionalized) and Zr-L3 ($-NO_2$ functionalized), for example, are taken up mostly by clathrin-mediated endocytosis and end up being degraded in the lysosomes, voiding their therapeutic effect. On the other hand, Zr-L5 and Zr-L6, although they are much less efficient at entering cells, are taken up through the caveolae-mediated route, allowing them to avoid lysosomal degradation, and to release their cargo in the desired intracellular location. Finally, we confirmed these findings by evaluating the therapeutic effect of each Zr-based MOF loaded with α-CHC, with the findings showing an enhanced effect of the drug when loaded within Zr-L6. All these results demonstrate the importance of designing a suitable and efficient drug delivery vector and the chemical flexibility that MOFs offer for this aim. For future experiments, the shape of particles may be included as a new variable, as it is another intrinsic characteristic of particles that affects the cellular uptake.[61,62]

ASSOCIATED CONTENT

Supporting Information

The Supporting Information is available free of charge on the ACS Publications website at DOI: 10.1021/acsami.7b07342.

Full experimental procedures, powder X-ray diffraction patterns of materials, SEM microscopy images, statistical analysis of results (PDF)

AUTHOR INFORMATION

Corresponding Authors

*E-mail: ross.forgan@glasgow.ac.uk.
*E-mail: df334@cam.ac.uk.

ORCID

Ross J. Marshall: 0000-0001-5756-0306
Inhar Imaz: 0000-0002-0278-1141
Daniel Maspoch: 0000-0003-1325-9161
Ross S. Forgan: 0000-0003-4767-6852
David Fairen-Jimenez: 0000-0002-5013-1194

Author Contributions

¶These authors contributed equally.

Notes

The authors declare no competing financial interest.

ACKNOWLEDGMENTS

C.A.O. thanks Becas Chile and the Cambridge Trust for funding. S.H. thanks the Cambridge Trust for funding. R.S.F. and D.F.-J. thank the Royal Society for the receipt of University Research Fellowships. D.F.-J. thanks financial support from ERC-2016-COG 726380. R.S.F., R.J.M., and I.A.L. thank the University of Glasgow and the EPSRC (EP/L004461/1) for funding. G.B., I.I., and D.M. acknowledge the financial support from 2014-SGR-80, MAT2015-65354-C2-1-R and EU FP7 ERC-Co 615954. ICN2 received support from the Spanish MINECO through the Severo Ochoa Centers of Excellence Program, under Grant No. SEV-2013-0295.

REFERENCES

(1) Parveen, S.; Misra, R.; Sahoo, S. K. Nanoparticles: A Boon to Drug Delivery, Therapeutics, Diagnostics and Imaging. *Nanomedicine* **2012**, *8* (2), 147−166.

(2) Moghimi, S. M.; Hunter, A. C.; Murray, J. C. Nanomedicine: Current Status and Future Prospects. *FASEB J.* **2005**, *19* (3), 311−330.

(3) De Jong, W. H.; Borm, P. Drug Delivery and Nanoparticles: Applications and Hazards. *Int. J. Nanomed.* **2008**, *3* (2), 133−149.

(4) Davis, M. E.; Chen, Z. G.; Shin, D. M. Nanoparticle Therapeutics: An Emerging Treatment Modality for Cancer. *Nat. Rev. Drug Discovery* **2008**, *7* (9), 771−782.

(5) Miller, S. E.; Teplensky, M. H.; Moghadam, P. Z.; Fairen-Jimenez, D. Metal-Organic Frameworks as Biosensors for Luminescence-Based Detection and Imaging. *Interface Focus* **2016**, *6*, 20160027.

(6) Furukawa, H.; Cordova, K. E.; O'Keeffe, M.; Yaghi, O. M. The Chemistry and Applications of Metal-Organic Frameworks. *Science* **2013**, *341* (6149), 1230444.

DOI: 10.1021/acsami.7b07342
ACS Appl. Mater. Interfaces 2017, 9, 35516−35525

(7) Horcajada, P.; Gref, R.; Baati, T.; Allan, P. K.; Maurin, G.; Couvreur, P.; Férey, G.; Morris, R. E.; Serre, C. Metal-Organic Frameworks in Biomedicine. *Chem. Rev.* **2012**, *112* (2), 1232−1268.
(8) Bernini, M. C.; Fairen-Jimenez, D.; Pasinetti, M.; Ramirez-Pastor, A. J.; Snurr, R. Q. Screening of Bio-Compatible Metal−organic Frameworks as Potential Drug Carriers Using Monte Carlo Simulations. *J. Mater. Chem. B* **2014**, *2* (7), 766−774.
(9) McKinlay, A. C.; Xiao, B.; Wragg, D. S.; Wheatley, P. S.; Megson, I. L.; Morris, R. E. Exceptional Behavior over the Whole Adsorption-Storage-Delivery Cycle for NO in Porous Metal Organic Frameworks. *J. Am. Chem. Soc.* **2008**, *130* (31), 10440−10444.
(10) He, C.; Lu, K.; Liu, D.; Lin, W. Nanoscale Metal-Organic Frameworks for the Co-Delivery of Cisplatin and Pooled siRNAs to Enhance Therapeutic Efficacy in Drug-Resistant Ovarian Cancer Cells. *J. Am. Chem. Soc.* **2014**, *136* (14), 5181−5184.
(11) Horcajada, P.; Chalati, T.; Serre, C.; Gillet, B.; Sebrie, C.; Baati, T.; Eubank, J. F.; Heurtaux, D.; Clayette, P.; Kreuz, C.; Chang, J.-S.; Hwang, Y. K.; Marsaud, V.; Bories, P.-N.; Cynober, L.; Gil, S.; Férey, G.; Couvreur, P.; Gref, R. Porous Metal-Organic-Framework Nanoscale Carriers as a Potential Platform for Drug Delivery and Imaging. *Nat. Mater.* **2010**, *9* (2), 172−178.
(12) Simon-Yarza, M. T.; Baati, T.; Paci, A.; Lesueur, L. L.; Seck, A.; Chiper, M.; Gref, R.; Serre, C.; Couvreur, P.; Horcajada, P. Antineoplastic Busulfan Encapsulated in a Metal Organic Framework Nanocarrier: First in Vivo Results. *J. Mater. Chem. B* **2016**, *4*, 585−588.
(13) Vasconcelos, I. B.; Silva, T. G.; Militão, G. C. G.; Soares, T. A.; Rodrigues, N. M.; Rodrigues, M. O.; Costa, N. B.; Freire, R. O.; Junior, S. A. Cytotoxicity and Slow Release of the Anti-Cancer Drug Doxorubicin from ZIF-8. *RSC Adv.* **2012**, *2* (25), 9437−9442.
(14) Zhu, X.; Gu, J.; Wang, Y.; Li, B.; Li, Y.; Zhao, W.; Shi, J. Inherent Anchorage in UiO-66 Nanoparticles for Efficient Capture of Alendronate and Its Mediated Release. *Chem. Commun.* **2014**, *50*, 8779−8782.
(15) Giménez-Marqués, M.; Hidalgo, T.; Serre, C.; Horcajada, P. Nanostructured Metal-Organic Frameworks and Their Bio-Related Applications. *Coord. Chem. Rev.* **2016**, *307*, 342−360.
(16) Orellana-Tavra, C.; Baxter, E. F.; Tian, T.; Bennett, T. D.; Slater, N. K. H.; Cheetham, A. K.; Fairen-Jimenez, D. Amorphous Metal-Organic Frameworks for Drug Delivery. *Chem. Commun.* **2015**, *51* (73), 13857−13992.
(17) Orellana-Tavra, C.; Marshall, R. J.; Baxter, E. F.; Lázaro, I. A.; Tao, A.; Cheetham, A. K.; Forgan, R. S.; Fairen-Jimenez, D. Drug Delivery and Controlled Release from Biocompatible Metal−organic Frameworks Using Mechanical Amorphization. *J. Mater. Chem. B* **2016**, *4*, 7697−7707.
(18) Orellana-Tavra, C.; Mercado, S. A.; Fairen-Jimenez, D. Endocytosis Mechanism of Nano Metal-Organic Frameworks for Drug Delivery. *Adv. Healthcare Mater.* **2016**, *5* (17), 2261−2270.
(19) Röder, R.; Preiß, T.; Hirschle, P.; Steinborn, B.; Zimpel, A.; Höhn, M.; Rädler, J. O.; Bein, T.; Wagner, E.; Wuttke, S.; Lächelt, U. Multifunctional Nanoparticles by Coordinative Self-Assembly of His-Tagged Units with Metal-Organic Frameworks. *J. Am. Chem. Soc.* **2017**, *139*, 2359.
(20) Abanades-Lazaro, I.; Haddad, S.; Sacca, S.; Orellana-Tavra, C.; Fairen-Jimenez, D.; Forgan, R. S. Selective Surface PEGylation of UiO-66 Nanoparticles for Enhanced Stability, Cell Uptake, and pH-Responsive Drug Delivery. *Chem.* **2017**, *2*, 561−578.
(21) Kou, L.; Sun, J.; Zhai, Y.; He, Z. The Endocytosis and Intracellular Fate of Nanomedicines: Implication for Rational Design. *Asian J. Pharm. Sci.* **2013**, *8* (1), 1−10.
(22) Mayor, S.; Pagano, R. E. Pathways of Clathrin-Independent Endocytosis. *Nat. Rev. Mol. Cell Biol.* **2007**, *8* (8), 603−612.
(23) Iversen, T.-G.; Skotland, T.; Sandvig, K. Endocytosis and Intracellular Transport of Nanoparticles: Present Knowledge and Need for Future Studies. *Nano Today* **2011**, *6* (2), 176−185.
(24) Park, J. H.; Oh, N. Endocytosis and Exocytosis of Nanoparticles in Mammalian Cells. *Int. J. Nanomed.* **2014**, *9* (9), 51−63.
(25) Kumari, S.; Mg, S.; Mayor, S. Endocytosis Unplugged: Multiple Ways to Enter the Cell. *Cell Res.* **2010**, *20* (3), 256−275.
(26) Dos Santos, T.; Varela, J.; Lynch, I.; Salvati, A.; Dawson, K. a. Effects of Transport Inhibitors on the Cellular Uptake of Carboxylated Polystyrene Nanoparticles in Different Cell Lines. *PLoS One* **2011**, *6* (9), e24438.
(27) Mellman, I. Endocytosis and Molecular Sorting. *Annu. Rev. Cell Dev. Biol.* **1996**, *12*, 575−625.
(28) Rejman, J.; Oberle, V.; Zuhorn, I. S.; Hoekstra, D. Size-Dependent Internalization of Particles via the Pathways of Clathrin- and Caveolae-Mediated Endocytosis. *Biochem. J.* **2004**, *377* (1), 159−169.
(29) Sevimli, S.; Sagnella, S.; Macmillan, A.; Whan, R.; Kavallaris, M.; Bulmus, V.; Davis, T. P. The Endocytic Pathway and Therapeutic Efficiency of Doxorubicin Conjugated Cholesterol-Derived Polymers. *Biomater. Sci.* **2015**, *3* (2), 323−335.
(30) McMahon, H. T.; Boucrot, E. Molecular Mechanism and Physiological Functions of Clathrin-Mediated Endocytosis. *Nat. Rev. Mol. Cell Biol.* **2011**, *12* (8), 517−533.
(31) Pelkmans, L.; Bürli, T.; Zerial, M.; Helenius, A. Caveolin-Stabilized Membrane Domains as Multifunctional Transport and Sorting Devices in Endocytic Membrane Traffic. *Cell* **2004**, *118* (6), 767−780.
(32) Guo, C.-J.; Wu, Y.-Y.; Yang, L.-S.; Yang, X.-B.; He, J.; Mi, S.; Jia, K.-T.; Weng, S.-P.; Yu, X.-Q.; He, J.-G. Infectious Spleen and Kidney Necrosis Virus (a Fish Iridovirus) Enters Mandarin Fish Fry Cells via Caveola-Dependent Endocytosis. *J. Virol.* **2012**, *86* (5), 2621−2631.
(33) Pelkmans, L.; Kartenbeck, J.; Helenius, A. Caveolar Endocytosis of Simian Virus 40 Reveals a New Two-Step Vesicular-Transport Pathway to the ER. *Nat. Cell Biol.* **2001**, *3* (5), 473−483.
(34) Gonzalez-Gaitan, M.; Stenmark, H. Endocytosis and Signaling: A Relationship under Development Meeting. *Cell* **2003**, *115*, 513−521.
(35) Damm, E. M.; Pelkmans, L.; Kartenbeck, J.; Mezzacasa, A.; Kurzchalia, T.; Helenius, A. Clathrin- and Caveolin-1-Independent Endocytosis: Entry of Simian Virus 40 into Cells Devoid of Caveolae. *J. Cell Biol.* **2005**, *168* (3), 477−488.
(36) Greim, H. Zirconium and Its Compounds, the MAK Collection for Occupational Health and Safety. In *Zirconium and Its Compounds*; The MAK Collection for Occupational Health and Safety, 1999; pp 224−236.
(37) Cunha, D.; Gaudin, C.; Colinet, I.; Horcajada, P.; Maurin, G.; Serre, C. Rationalization of the Entrapping of Bioactive Molecules into a Series of Functionalized Porous Zirconium Terephthalate MOFs. *J. Mater. Chem. B* **2013**, *1* (8), 1101−1108.
(38) Cavka, J. H.; Jakobsen, S.; Olsbye, U.; Guillou, N.; Lamberti, C.; Bordiga, S.; Lillerud, K. P. A New Zirconium Inorganic Building Brick Forming Metal Organic Frameworks with Exceptional Stability. *J. Am. Chem. Soc.* **2008**, *130* (42), 13850−13851.
(39) Katz, M. J.; Brown, Z. J.; Colón, Y. J.; Siu, P. W.; Scheidt, K. A.; Snurr, R. Q.; Hupp, J. T.; Farha, O. K. A Facile Synthesis of UiO-66, UiO-67 and Their Derivatives. *Chem. Commun.* **2013**, *49* (82), 9449−9451.
(40) Cmarik, G. E.; Kim, M.; Cohen, S. M.; Walton, K. S. Tuning the Adsorption Properties of UiO-66 via Ligand Functionalization. *Langmuir* **2012**, *28* (44), 15606−15613.
(41) Marshall, R. J.; Hobday, C. L.; Murphie, C. F.; Griffin, S. L.; Morrison, C. A.; Moggach, S. A.; Forgan, R. S. Amino Acids as Highly Efficient Modulators for Single Crystals of Zirconium and Hafnium Metal−organic Frameworks. *J. Mater. Chem. A* **2016**, *4* (18), 6955−6963.
(42) Orellana-Tavra, C.; Baxter, E. F.; Tian, T.; Bennett, T. D.; Slater, N. K. H.; Cheetham, A. K.; Fairen-Jimenez, D. Amorphous Metal−organic Frameworks for Drug Delivery. *Chem. Commun.* **2015**, *51* (73), 13878−13881.
(43) Nazarenus, M.; Zhang, Q.; Soliman, M. G.; del Pino, P.; Pelaz, B.; Carregal-Romero, S.; Rejman, J.; Rothen-Rutishauser, B.; Clift, M. J. D.; Zellner, R.; Nienhaus, G. U.; Delehanty, J. B.; Medintz, I. L.; Parak, W. J. In Vitro Interaction of Colloidal Nanoparticles with

DOI: 10.1021/acsami.7b07342
ACS Appl. Mater. Interfaces 2017, 9, 35516−35525

Mammalian Cells: What Have We Learned Thus Far? *Beilstein J. Nanotechnol.* **2014**, *5* (1), 1477−1490.
(44) Oliver, A. E.; Jamil, K.; Crowe, J. H.; Tablin, F. Loading Human Mesenchymal Stem Cells with Trehalose by Fluid-Phase Endocytosis. *Cell Preserv. Technol.* **2004**, *2* (1), 35−49.
(45) Ivanov, A. I. *Exocytosis and Endocytosis*; Walker, J. M., Ed.; Human Press, 2008.
(46) Sarkar, K.; Kruhlak, M. J.; Erlandsen, S. L.; Shaw, S. Selective Inhibition by Rottlerin of Macropinocytosis in Monocyte-Derived Dendritic Cells. *Immunology* **2005**, *116* (4), 513−524.
(47) Stamatovic, S. M.; Keep, R. F.; Wang, M. M.; Jankovic, I.; Andjelkovic, A. V. Caveolae-Mediated Internalization of Occludin and Claudin-5 during CCL2-Induced Tight Junction Remodeling in Brain Endothelial Cells. *J. Biol. Chem.* **2009**, *284* (28), 19053−19066.
(48) Inal, J.; Miot, S.; Schifferli, J. A. The Complement Inhibitor, CRIT, Undergoes Clathrin-Dependent Endocytosis. *Exp. Cell Res.* **2005**, *310* (1), 54−65.
(49) Yao, D.; Ehrlich, M.; Henis, Y. I.; Leof, E. B. Transforming Growth Factor-B Receptors Interact with AP2 by Direct Binding to B2 Subunit. *Mol. Biol. Cell* **2002**, *13* (11), 4001−4012.
(50) Carpentier, J. L.; Sawano, F.; Geiger, D.; Gorden, P.; Perrelet, a.; Orci, L. Potassium Depletion and Hypertonic Medium Reduce "Non-Coated" and Clathrin-Coated Pit Formation, as Well as Endocytosis through These Two Gates. *J. Cell. Physiol.* **1989**, *138* (3), 519−526.
(51) Fröhlich, E. The Role of Surface Charge in Cellular Uptake and Cytotoxicity of Medical Nanoparticles. *Int. J. Nanomed.* **2012**, *7*, 5577−5591.
(52) Harush-Frenkel, O.; Rozentur, E.; Benita, S.; Altschuler, Y. Surface Charge of Nanoparticles Determines Their Endocytic and Transcytotic Pathway in Polarized MDCK Cells. *Biomacromolecules* **2008**, *9* (2), 435−443.
(53) Rabinovich-Guilatt, L.; Couvreur, P.; Lambert, G.; Dubernet, C. Cationic Vectors in Ocular Drug Delivery Cationic Vectors in Ocular Drug Delivery. *J. Drug Target.* **2004**, *12* (9−10), 623−633.
(54) Dausend, J.; Musyanovych, A.; Dass, M.; Walther, P.; Schrezenmeier, H.; Landfester, K.; Mailander, V. Uptake Mechanism of Oppositely Charged Fluorescent Nanoparticles in HeLa Cells. *Macromol. Biosci.* **2008**, *8*, 1135−1143.
(55) Harush-frenkel, O.; Debotton, N.; Benita, S.; Altschuler, Y. Targeting of Nanoparticles to the Clathrin-Mediated Endocytic Pathway. *Biochem. Biophys. Res. Commun.* **2007**, *353*, 26−32.
(56) Wu, H.; Chua, Y. S.; Krungleviciute, V.; Tyagi, M.; Chen, P.; Yildirim, T.; Zhou, W. Unusual and Highly Tunable Missing-Linker Defects in Zirconium Metal−Organic Framework UiO-66 and Their Important Effects on Gas Adsorption. *J. Am. Chem. Soc.* **2013**, *135*, 10525.
(57) Okamoto, C. T. Endocytosis and Transcytosis. *Adv. Drug Delivery Rev.* **1998**, *29*, 215−228.
(58) Shin, J.-S.; Abraham, S. N. Caveolae as Portals of Entry for Microbes. *Microbes Infect.* **2001**, *3* (9), 755−761.
(59) Manders, E. M. M.; Verbeek, F. J.; Aten, J. A. Measurement of Co-Localization of Objects in Dual-Colour Confocal Images. *J. Microsc.* **1993**, *169*, 375−382.
(60) Bolte, S.; Cordelieres, F. P. A Guided Tour into Subcellular Colocalization Analysis in Light. *J. Microsc.* **2006**, *224*, 213−232.
(61) Chithrani, B. D.; Chan, W. C. W. Elucidating the Mechanism of Cellular Uptake and Removal of Protein-Coated Gold Nanoparticles of Different Sizes and Shapes. *Nano Lett.* **2007**, *7* (6), 1542−1550.
(62) Chithrani, B. D.; Ghazani, A. A.; Chan, W. C. W. Determining the Size and Shape Dependence of Gold Nanoparticle Uptake into Mammalian Cells. *Nano Lett.* **2006**, *6* (4), 662−668.

DOI: 10.1021/acsami.7b07342
ACS Appl. Mater. Interfaces 2017, 9, 35516−35525